

Control Of PV Charger System With SEPIC Converter

A. Giddaiah P.G Student, K. Kishore Reddy asst. Professor,

RGM CET, Nandyal
Dept. of EEE, RGM CET, Nandyal,

Abstract

The photovoltaic (PV) stand-alone system requires a battery charger for energy storage. This paper presents the modeling and controller design of the PV charger system implemented with the single-ended primary inductance converter (SEPIC). The designed SEPIC employs the peak-current-mode control with the current command generated from the input PV voltage regulating loop, where the voltage command is determined by both the PV module maximum power point tracking (MPPT) control loop and the battery charging loop. The control objective is to balance the power flow from the PV module to the battery and the load such that the PV power is utilized effectively and the battery is charged with three charging stages. This paper gives a detailed modeling of the SEPIC with the PV module input and peak-current-mode control first. Accordingly, the PV voltage controller, as well as the adaptive MPPT controller, is designed. An 80-W prototype system is built. The effectiveness of the proposed methods is proved with some simulation and experimental results.

Index Terms—Maximum power point tracking (MPPT), power balance control, single-ended primary inductance converter (SEPIC), stand-alone.

I. INTRODUCTION

SOLAR POWER is more and more attractive due to theseverer environmental protection regulation and the predictable shortage of conventional energy sources. As a result, many research works have addressed the development of solar power system in recent years. Many types of photovoltaic (PV) power conversion systems have been developed including the grid-connected system for reducing the power from the utility and the stand-alone system for providing the load power without the utility. The stand-alone system requires battery for energy storage to supply the load power during the period without or shortage of solar power. Because the $P-V$ characteristic of the PV module is varied with the insulation level as well as the temperature, if the peak power voltage of the PV module does not match with the battery voltage, the energy conversion efficiency of the PV module will be reduced using the direct connection of the PV module and the battery. Therefore, a battery charger is required to track the peak power of the PV module

in all operation conditions. In addition, the battery charging needs control for achieving high state of charge (SOC) and, consequently, longer lifetime of the battery.

This paper explores the charger system implemented with the single-ended primary inductance converter (SEPIC). Although the boost converter usually has higher efficiency than the SEPIC, however, it is only applicable for cases where the battery voltage is higher than the PV module voltage. The buck-boost feature of the SEPIC widens the applicable PV voltage and thus increases the adopted PV module flexibility.

The comparison of various buck-boost converters from different points of view is shown in Table I. Among these converters, although the SEPIC is not the best from the views of efficiency and cost, it still has the merits of non-inverting polarity, easy-to-drive switch, and low input-current pulsating for high-precise MPPT that makes its integral characteristics suitable for the low-power PV charger system. This paper will investigate the SEPIC with the PV module input and the peak-current-mode control that was seldom presented in previous studies. The small-signal model of such a SEPIC will be derived, and upon which, the PV voltage controller and the MPPT controller will be designed.

Another important issue of the PV charger system is the power balance control that was faced commonly for multiple source system, such as fuel-cell hybrid vehicle, hybrid PV and fuel-cell power system hybrid wind, solar, and distributed-generation power system and so on. For the PV charger system, MPPT and battery charging must be cooperative, and the load demand must be considered simultaneously such that the PV power can be utilized effectively and the battery is suitably charged. Jiang and Dougal. Treat this issue as a multiobjective problem. It classifies the system into various states based on the operating conditions of the PV module, the battery, and the load. By judging the state and setting the related control goal, the power will be balanced to satisfy the MPPT control and battery charging requirement. However, the multiobjective control algorithm requires sense of many states and sophisticated state judgment, and thus, needs software programming. This paper will present a power balance control method that achieves the same functions as that in but with only a simple control circuit. In addition,

the proposed power balance control can also be extended to the system with more sources like those shown in . Furthermore, all power sources can be utilized with the preset priority based on their importance to the system.

An 80-W prototype charger system implemented with some analog circuits and Matlab real-time control is designed and built. The effectiveness of the proposed system is proved with some PSIM simulation and experimental results.

TABLE I
COMPARISON OF VARIOUS BUCK-BOOST CONVERTERS

| Converters | Buck-boost | Cuk | Positive Buck-boost [13] | SEPIC | Flyback |
|-------------------------|---------------------------|--|--|--|---|
| Output voltage Polarity | Invert | Invert | Non-invert | Non-invert | Non-invert |
| Input current | Pulsating | Nonpulsating | Depends on operation mode | Nonpulsating | Pulsating |
| Switch drive | Floated | Floated | One floated One grounded | Grounded | Grounded |
| Efficiency | Low | Medium | High with only one stage is active | Medium | Low |
| Cost | Medium due to float drive | Medium due to additional block capacitor | High due to an additional switch and diode, a more complex drive circuit | Medium due to additional block capacitor | Low due to grounded switch and no block capacitor |

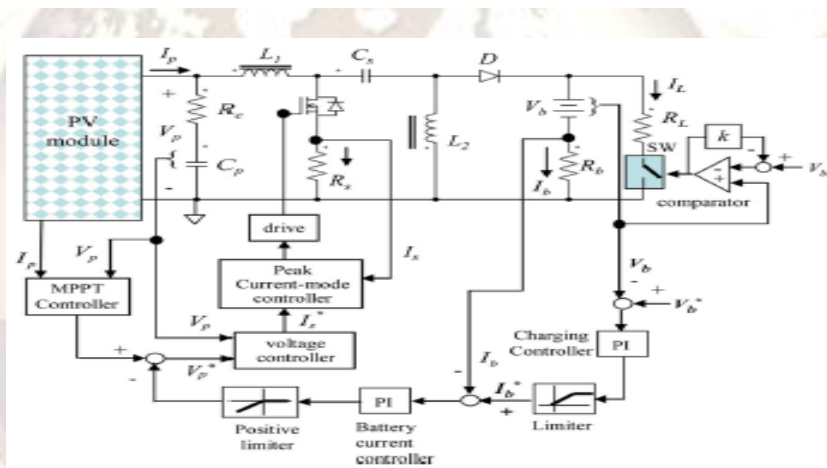


Fig. 1. Circuit configuration of the proposed PV charger

II. CIRCUIT CONFIGURATION AND POWER BALANCE CONTROL OF THE CHARGER

The circuit configuration of the proposed PV charger is shown in Fig. 1. The SEPIC converter employs the peak current-mode control with an outer PV voltage regulating loop, where the voltage command (V_p^*) is generated by combining the MPPT control loop and the battery charging loop. The combination of MPPT and charging control is for instantaneously balancing the system power to charge the battery with three stages, namely, constant-current, constant-voltage, and floating charge stages.

Based on the PV power generation, the battery SOC, and the load condition, the designed controller shown in Fig. 1 can operate the system in three operation modes, as shown in Fig. 2. Fig. 2(a) shows the discharging mode wherein the available maximum PV power is less than the load power. The insufficient power will be automatically supplied by the discharge of the battery. Fig. 2(b) shows the

partial charging mode wherein the available maximum PV power is larger than the load power and the excessive power will charge the battery, but the charging current is still less than the preset charge current command (I_b^*). In the aforementioned two modes, because the battery current (I_b) in Fig. 1 cannot reach its current command (I_b^*) the signal generated by the battery current controller that is a proportional and integral (PI) controller will go positive and be limited to be zero. It results that the voltage command (V_p^*) is determined completely by the MPPT controller, and thus, the PV module is operated in the MPPT point, as shown in Fig. 2(a) and (b). As the available peak power of the PV module is larger than the battery charging and load requirement, the battery current in Fig. 1 will reach its command (I_b^*), and the signal generated by the battery current controller will go negative and will now add voltage to increase the voltage command generated by the MPPT controller. As a result, the PV module will discard the MPPT because the

voltage command (V_p^*) is shifted to a higher level than the MPPT voltage, and finally, the generated PV power will balance the load and charging requirement in the charging mode shown in Fig. 2(c).

The charging controller is a PI controller. The limiter behind the charging controller will set the charging current command (I_b^*) to be a maximum charging current level as the battery voltage (V_b) has not reached its maximum charged voltage command (V_b^*). In this case, and if the power condition is sufficient as Fig. 2(c), the system will operate in the constant current charge stage. As the battery voltage approximately reaches the voltage command (V_b^*), the limiter will enter the linear region, and the charging current command (I_b^*) will reduce. This stage is called the constant-voltage charge stage. Finally, as the battery voltage reaches the voltage command (V_b^*) and the limiter output (I_b^*) is reduced to be approximately zero

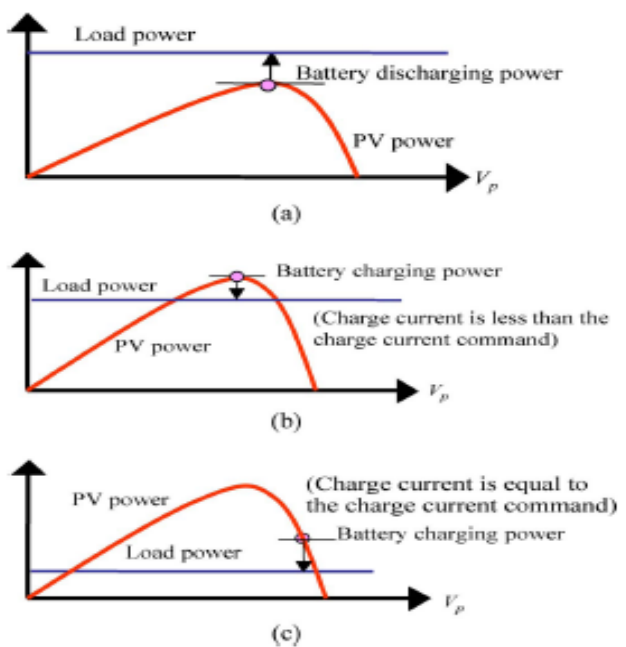


Fig. 2. Operation modes of the charger system. (a) Discharging mode. (b) Partial charging mode. (c) Charging mode.

the battery is in the floating-charge stage, i.e., the fully SOC.

Through the proposed control arrangement, the PV module will operate at MPPT, and the MPPT is discarded only when the available PV power is larger than the total power for battery charge and supplying the load. This is the most effective way for utilizing the PV power. In addition, the battery will not be overcharged and will stay at a high SOC voltage level if the PV power is enough. On the other hand, to guarantee no over discharge of the battery as the PV power is insufficient, a load switch controlled with a hysteric comparator is used in Fig. 1 to disconnect the load as the battery voltage is lower

than a low SOC level and reconnect the load if the battery voltage is larger than a safety level (V_{bl}^*) higher than the low SOC level. The proposed power balance control method shown in Fig. 1 can be easily extended to the system with more sources. Fig. 3 shows the extension that two PV charge circuits charge the same battery, and the related operation modes are shown in Fig. 4. By passing the signal (V_L) generated by the positive limiter to the negative limiter, the V_L signal can be distributed to be two as V_{L1} and V_{L2} . These two signals are then used to correct the signals generated by both MPPT controllers to produce the PV voltage commands for both chargers as that done in Fig. 1. If the positive limiter's output is zero, then both MPPT controllers will not be affected by the charge controller, and both PV modules will be at MPPT. The operation modes shown in Fig. 4(a) and (b) both belong to this case. If the positive limiter's output is negative and is not limited by the negative limiter, V_{L2} will be zero, and V_{L1} will shift the MPPT of PV module 1. Therefore, PV module 2 is at MPPT, but PV module 1 is not, as shown in Fig. 4(c). If the positive limiter's output is negative and limited by the negative limiter, V_{L2} will not be zero. V_{L1} and V_{L2} will shift the MPPT of both PV modules. If the level of V_{L1} exactly shifts PV module 1 to be the open circuit voltage, then the total power is only contributed by PV module 2, as shown in Fig. 4(d). The power balance control method shown in Fig. 3 can also be applied to the system with more sources just by distributing the signal V_L . It allows the sources with different power characteristics. In addition, the power source utilization can be assigned with priority, as done in Fig. 3, where PV module 2 will be utilized first and then PV module 1. This feature is not proposed by all previous studies .

III. MODELING AND CONTROLLER DESIGN OF CHARGER

SEPIC is a buck-boost-derived converter that possesses a right-half-plane (RHP) zero in the continuous conduction mode (CCM), even with the peak-current-mode control in the output voltage regulation mode . Following the averaged switch modeling technique presented in the control-to-output transfer function of the SEPIC in CCM with output-voltage regulation can be derived from Fig. 1 to be the following form:

$$\frac{\tilde{V}_B}{\tilde{D}} \Big|_{\tilde{V}_P = \tilde{V}_{Cs} = 0} = \frac{V_P - V_B}{D^2} \frac{(1 - s \frac{DL}{D'R_L})}{(1 + s \frac{L}{D^2 R_L} + s^2 \frac{LC_C}{D'^2})} \quad (1)$$

where D is the duty ratio of the switch, with $D' = 1 - D$.

Here, for deriving from Fig. 1, the battery is changed to be an output-filter capacitor C_o , the input voltage V_p is changed to be a constant-voltage source,

and the inductors are set to be $L_1 = L_2 = L$ for simplification. Equation (1) possesses an RHP zero located at $D'RL/(DL)$. Opposite to output voltage regulation as the conventional converter, the proposed PV charger regulates the input voltage. The CCM operation is preferred here for reducing the input-current ripple and reduced the switch-current stress. As will be seen in the following, opposite to the output-voltage capacitor charged by the diode current of the output regulation structure, there is no RHP zero problem of the proposed PV charger because the input capacitor current is charge controlled with the input inductor current, and the input is a PV current source for the input regulation structure. In the following, the analysis and design are based on the CCM operation mode.

A. DESIGN OF POWER CIRCUIT

Referring to Fig. 1, the voltage transfer ratio of the SEPIC inCCM is

$$M = \frac{V_B}{V_P} = \frac{D}{1-D} \quad (2)$$

where D is the duty ratio of the switch. If the input inductor is designed based on the idea that the SEPIC is operated in CCM within the prescribed power range, then the input inductor L_1 will satisfy the following relation:

$$\Delta i_{L1,pp} = 2I_{p,min} = \frac{2P_{pv,min}}{V_p} = \frac{V_p}{L_1} D_{max} T_s \quad (3)$$

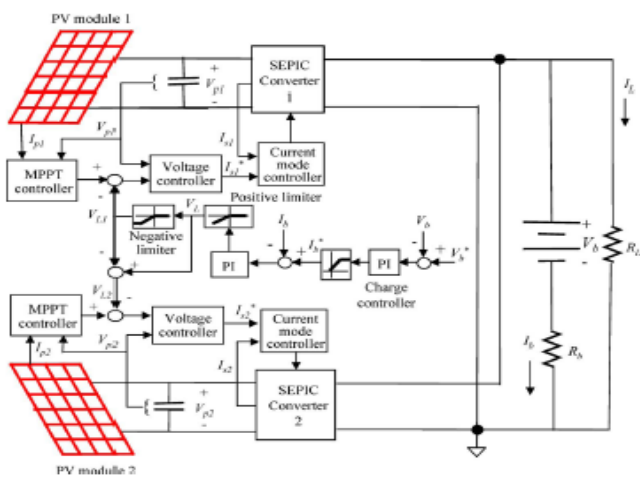


Fig. 3. Proposed power balance control method applied for two PV charger systems.

where $\Delta i_{L1,pp}$ is the peak-to-peak value of the input inductor current. $P_{pv,min}$ is the prescribed minimum PV power. $I_{p,min}$ is the PV module current corresponding to $P_{pv,min}$. The inductor L_2 is designed to couple with L_1 as a flyback transformer to reduce the volume. The turn ratio is one ($L_1 = L_2$) to make both inductors enter into CCM simultaneously. Substituting (2) into (3) results in

$$L_1 = L_2 = \frac{V_B^2}{2M(M+1)P_{pv,min}f_s} \quad (4)$$

The input-voltage ripple is caused by the charge and discharge of the capacitor C_s , as well as the ripple caused by the equivalent series resistance (ESR) of the capacitor. The electrolytic capacitor having non negligible ESR is adopted here, and the input-voltage ripple is caused mainly by it at the adopted switching frequency (40 kHz). As a result, the input capacitor is selected based on the ESR value (R_e) and the voltage ripple demand (ΔV_p) as

$$R_e = \frac{\Delta V_p}{\Delta i_{L1,pp}} = \frac{\Delta V_p}{2I_{p,min}} \quad (5)$$

Once ESR is determined, the capacitance (C_p) can be designed from the datasheet of the capacitor. The voltage ripple is specified with the precision of the MPPT. A larger ripple will render a larger fluctuation around the MPPT operation point. As for the coupling capacitor C_s , it has to flow the maximum input current pulse, and a small ESR is required for reducing the loss. In this paper, it is selected to be the same as the input capacitor C_p .

It should be noted that if the switching frequency of the converter is high enough such that the capacitance of the input capacitor can be reduced significantly, the tantalum and the ceramic capacitors with lower ESR can be adopted cost effectively. The design of capacitor can then be changed to be with charge and discharge of the capacitor but not with the ESR.

B. MODELING AND CONTROL OF SEPIC

The equivalent circuit of the PV cell is shown in Fig. 5

where R_{sh} and R_s are the intrinsic shunt and series resistances of the cell, respectively. Usually, the value of R_{sh} is very large, and that of R_s is very small; hence, they may be neglected to simplify the analysis. PV cells are grouped in larger units called PV modules which are further interconnected in a parallel-series configuration to form PV arrays. The PV array mathematical model can be represented as follows

$$I_p = n_p I_{ph} - n_p I_{sat} \left[\exp \left(\frac{q}{KAT} \frac{V_p}{n_s} \right) - 1 \right] \quad (6)$$

where I_p is the PV module array output current (in amperes), V_p is the PV array output voltage, n_s is the number of modules connected in series, n_p is the number of modules connected in parallel, q is the charge of an electron, K is Boltzmann's constant, A is the p-n junction ideality factor, T is the cell temperature (in kelvins), and I_{sat} is the cell reverse saturation current. The peak-current-mode control with input PV voltage regulation of the SEPIC is shown in Fig. 6(a), where the PV module is represented as a current source modeled by (6), with

$n_s = n_p = 1$. The PV input power is

$$P_{PV} = VI_p \tag{7}$$

Under a fixed insolation condition, a small perturbation of (7) can be found as

$$\bar{P}_{PV} = \bar{V}I_p + \bar{I}_pV \tag{8}$$

Equation (8) can be rearranged to represent the small-signal expression of the PV module current

$$\bar{I}_p = \frac{-I_p}{V}\bar{V} + \frac{\bar{P}_{PV}}{V} \tag{9}$$

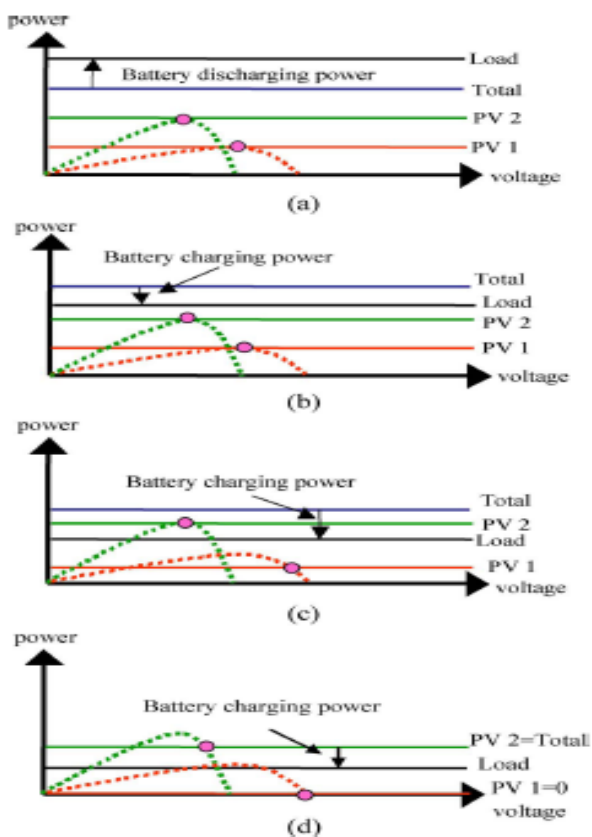


Fig. 4. Operation modes of two PV charger systems. (a) Discharging mode. (b) Partial charging mode. (c) Charging mode with PV module 1 not at MPPT. (d) Charging mode with two PV modules not at MPPT.

One can obtain the input capacitor current from Fig. 6(a) as

$$C_p \frac{dV}{dt} = I_p - I_{L1} \tag{10}$$

The small-signal expression of (10) is

$$C_p \frac{d\bar{V}}{dt} = \bar{I}_p - \bar{I}_{L1} \tag{11}$$

Substituting (9) into (11) yields

$$C_p \frac{d\bar{V}}{dt} = \frac{-I_p}{V}\bar{V} + \frac{\bar{P}_{PV}}{V} - \bar{I}_{L1} \tag{12}$$

The transfer function of the inductor current I_{L1} to the voltage V can be found from (12) as

$$\left. \frac{V(s)}{I_{L1}(s)} \right|_{\bar{P}_{PV}=0} = -\frac{R_p}{1 + sC_pR_p}, \quad R_p = \frac{V}{I_p} \approx \frac{V_p}{I_p} \tag{13}$$

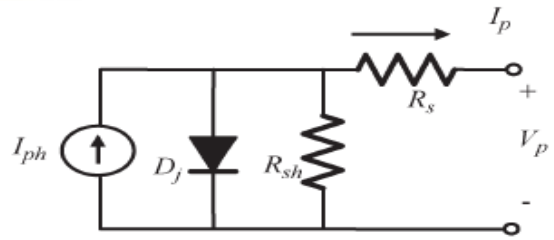


Fig. 5. Equivalent circuit of the PV cell.

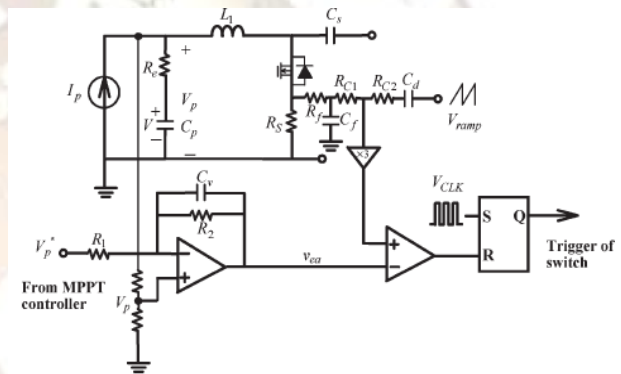


Fig. 6. Feedback control of the SEPIC

where R_p is the equivalent load resistor seen by the PV module. The relation between V and V_p can be found by considering the ESR of the capacitor as

$$\tilde{V} + R_e C_p \frac{d\tilde{V}}{dt} = \tilde{V}_p \tag{14}$$

The transfer function from I_{L1} to V_p can be found by combining (13) and the transfer function of (14) as

$$H(s) = \left. \frac{V_p(s)}{I_{L1}(s)} \right|_{\tilde{P}_{PV}=0} = -\frac{R_p(1 + sC_pR_e)}{1 + sC_pR_p} \tag{15}$$

includes a pole and a zero. The pole is determined by the capacitor C_p and the equivalent load resistor R_p . As compared with that in (1), the zero here is determined by C_p and the ESR value R_e that is a left-half-plane (LHP) zero. The UC3846 control IC is adopted for realizing the peak-current-mode control. The switch current is sensed with the resistor R_s . A low-pass filter formed by R_f - C_f is added to reduce the leading-edge spike caused by the discharge of the internal capacitor of the switch and the diode

recovery current. The slope compensation signal is added to the sensed current to prevent the subharmonic oscillation, as the duty cycle is larger than 0.5. The slope compensation signal is provided by the ramp signal coupled with a capacitor C_d . The level of compensation is adjusted with the ratio of resistors R_{c1} and R_{c2} . The compensated current signal is amplified three times and then compared with the voltage error signal V_{ea} of the voltage controller to reset the flip-flop which is set pulse by pulse by the clock signal v_{CLK} and to finally determine the duty ratio of the switch. Because the peak current of the inductor L_1 is the same as that of the switch, the transfer function from V_{ea} to I_{L1} can be found as

$$K = \frac{I_{L1}(s)}{V_{ea}(s)} = \frac{1}{3R_s \left(1 + \frac{m_a}{m_1}\right)} \quad (16)$$

where m_1 and m_a are the slopes of the sensed current and the compensated signal, respectively. For assuring a stable current loop under any PV voltage, $m_a/m_1 \geq 0.5$ is chosen. Combining (15) and (16), the transfer function of the voltage loop can be derived as

$$\frac{v_p(s)}{V_{ea}(s)} = P(s) = k_v k_H(s) = -\frac{\frac{k_v R_e}{3R_s \left(1 + \frac{m_a}{m_1}\right)} \left(s + \frac{1}{C_p R_e}\right)}{s + \frac{1}{C_p R_p}} \quad (17)$$

where v_p is the sensed PV voltage (V_p). The voltage sensing factor is k_v . The negative gain in (17) desires a positive feedback control of the input voltage. The low-pass filter, as in the following, is adopted as the compensator of the voltage controller

$$G_v(s) = \frac{V_c}{V_o} = \frac{\frac{1}{R_1 C_v}}{s + \frac{1}{C_v R_2}} \quad (18)$$

Its pole is designed to cancel the zero of (17), i.e., $R_2 C_v = R_e C_p$. Considering that the gain and the pole of (17) will drift with the PV voltage, the gain R_2/R_1 of the error amplifier should be designed to satisfy the stability and provide a suitable bandwidth of the voltage loop.

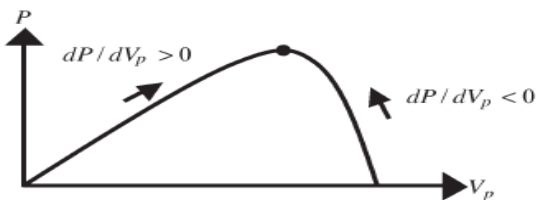


Fig.7. Adopted incremental conductance MPPT control algorithm.

C. MPPT CONTROLLER DESIGN

The proposed MPPT controller tracks the peak power of the PV module based on the power-voltage ($P-V_p$) characteristic shown in Fig. 7 and the

incremental conductance algorithm. In the positive-slope region ($dP/dV_p > 0$), the operation voltage is increased. On the other hand, in the negative slope region ($dP/dV_p < 0$), the operation voltage is decreased. The peak power point starting from any operating point will be finally reached through a few steps of voltage adjustment. In this paper, for increasing the tracking speed as well as the precision, the voltage adjusting speed is slope dependent. In the positive-slope region, the adjusting speed will be slower than the negative-slope region because the positive slope is smaller than the negative slope in amplitude. The adjusting speed will be slowed down near the peak power point. This is effective to prevent the tracking oscillation near the peak power point to increase the MPPT precision. The aforementioned MPPT control algorithm implemented with the Matlab real-time control (the details will be described in Section IV) is shown in Fig. 8. For avoiding error adjustment caused by the voltage and current ripples, the voltage and power are processed using a fourth moving-average filter before the slope calculation. The slope $\Delta P/\Delta V_p$ is calculated and then multiplied by a gain (Gain 1) and limited by a limiter (Limiter 1) to find the direction and set the voltage change in each step. The direction value is accumulated with a memory and then scaled with Gain 2 to fit the required voltage range. To make the MPPT start from the open-circuit voltage, the Init voltage nearing the open-circuit voltage is adopted to set the initial voltage command before the start of the converter. The voltage command is finally limited by Limiter 2 to limit the attainable PV voltage.

IV. IMPLEMENTATION AND VERIFICATION

An 80-W PV charger system is designed and built and tested with a 75-W Siemens SP75 PV module in this paper. The specification of the SEPIC is listed as follows:

$$\begin{aligned} V_p &= 10 \sim 22 \text{ V} & V_B &= 12 \text{ V} & f_s &= 40 \text{ kHz} \\ k_v &= 0.1 & R_s &= 0.05 & V_B &= 12 \text{ V} \\ P_{pv,min} &= 10 \text{ W} & I_{p,min} &= 0.5 \text{ A} & \Delta V_p &= 0.2 \text{ V}. \end{aligned} \quad (19)$$

$$M = \left(\frac{V_B}{V_p}\right)_{\max} = \frac{12}{10} = \frac{D_{\max}}{1 - D_{\max}}, \quad D_{\max} = 0.545. \quad (20)$$

The inductor value is then calculated with (4) as $L_1 = L_2 = 68 \mu\text{F}$. With the specification of ΔV_p and (5), the required $R_e = 0.2 \Omega$. Accordingly, the capacitor is found as

$$C_p = \frac{40 \times 10^{-6}}{R_e} = 200 \mu\text{F} \quad (21)$$

where 40×10^{-6} can be determined from the capacitor datasheet. The typical value is $30-80 \times 10^{-6}$. The real value of C_p is $220 \mu\text{F}$ in this paper.

The coupling capacitor C_s has the same value as the C_p . The voltage controller in (18) is designed with (17). However, the parameters in (17) are varied with the operating point of the PV module. For considering this factor, Fig. 9 shows five $P-V$ curves of the SP75 module corresponding to the cases of PV peak powers of 75, 60, 40, 30, and 10W, respectively. Three lines on the right side of each curve are chosen to calculate the equivalent output resistor value (R_p) of the PV module. The resistor value is determined

based on the slope of the $V-I$ curve. The voltage controller in (18) is then designed based on (17) and these resistor values. The MPPT in 75 W (R_{p1}) is adopted as the nominal case. The design procedure is as follows: 1) Set the crossover frequency (f_c) to be one-tenth of the switching frequency (f_s); 2) find the value $R_2/R_1=1/KH(f_c)$; 3) assign R_1 and then calculate R_2 with the ratio R_2/R_1 ; and 4) set the pole to be $R_2C_v=C_pR_e$ and then find C_v . The designed result of G_v is shown in Fig:10,

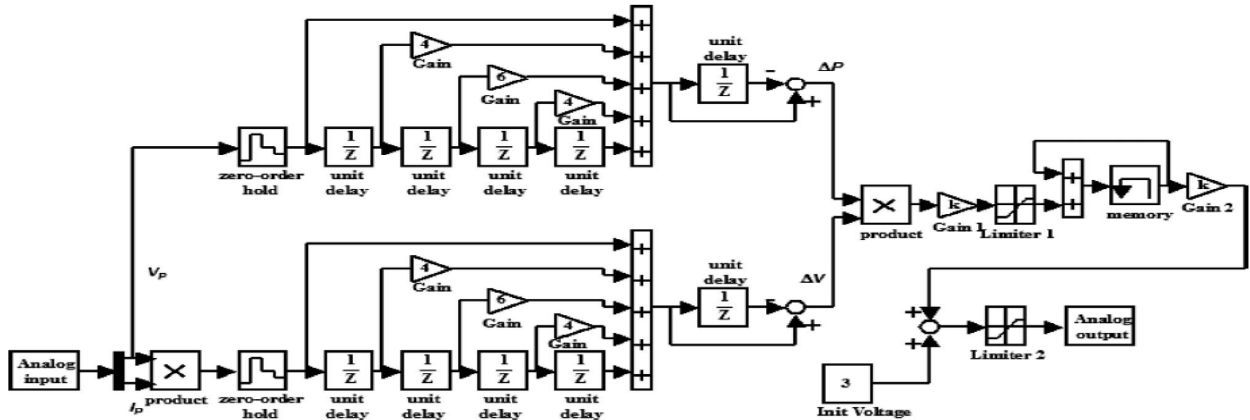


Fig. 8. Proposed MPPT control algorithm implemented with the Matlab real-time control.

in which the bode plots of $P(s)$ in with various values of R_p and the closed-loop response (G_vP) of the nominal case are also provided. The closed-loop response of the nominal case satisfies the aforementioned design. It can be examined that the closed-loop response for various cases is also stable.

The whole system is verified with the PSIM simulation first before implementation. It is constructed based on the aforeasaid design. For verifying the circuit modeling, the open-loop response of the voltage loop in the aforementioned nominal case is ac swept with the PSIM simulation, as shown in Fig. 11(a), in which the PV module is modeled as a voltage-controlled current source possessing the prescribed SP75 module $V-I$ curve. The current command is set to satisfy the 75-W input. Fig. 11(b) shows the sweep of the voltage loop that is closed further. The sweep results are very close to the theoretic results shown in Fig. 10, confirming the previous modeling and controller design.

The implementation of the whole system in the developing stage is shown in Fig. 12. The MPPT controller of the SEPIC charger is implemented with the Matlab real-time control on PC; other circuits of the SEPIC are implemented with the analog circuit. Fig. 13 shows the measured MPPT response at 50W. The waveforms of the PV module voltage and current and the $P-V$ trace prove that the response of the proposed MPPT

controller is fast. The precision of the MPPT controller is found to be up to 99.2% even at low PV power.

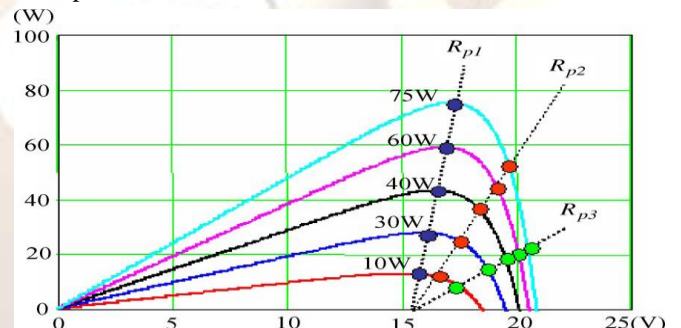
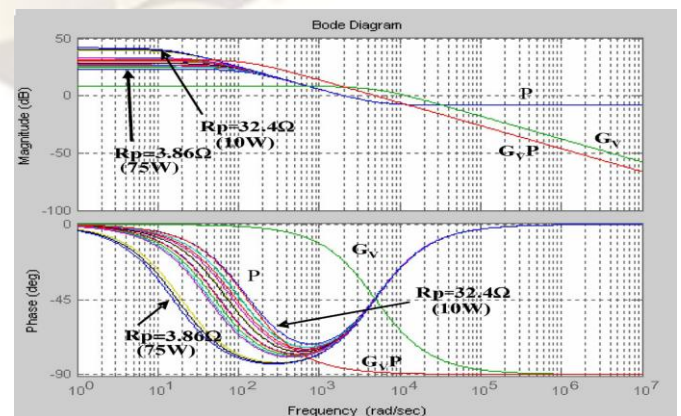


Fig. 9. Five $P-V$ curves corresponding to the cases of PV peak power of 75, 60, 40, 30, and 10 W, respectively.



10. Open- and closed-loop responses of the voltage.

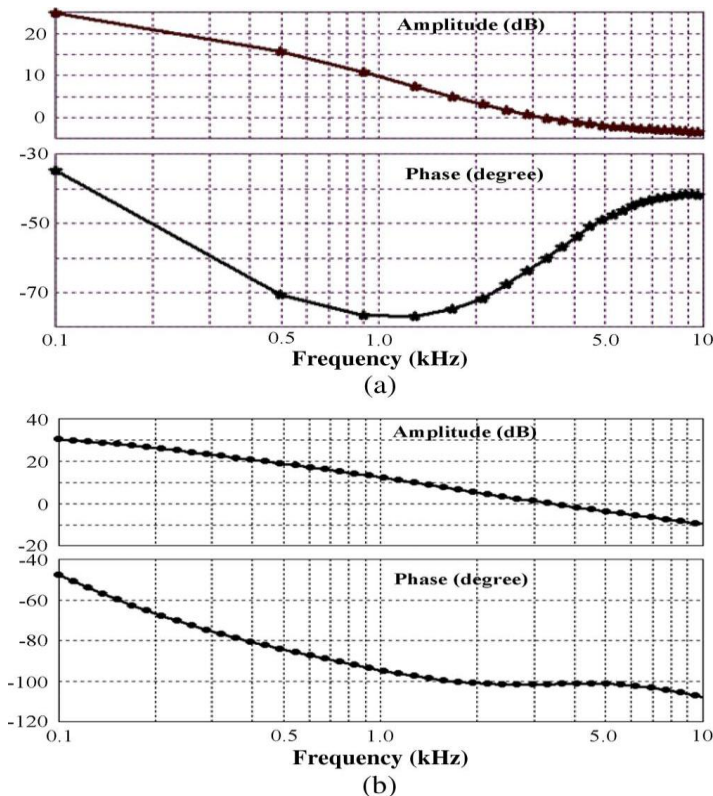


Fig. 11. AC sweep of the voltage loop. (a) Open loop. (b) Closed loop.

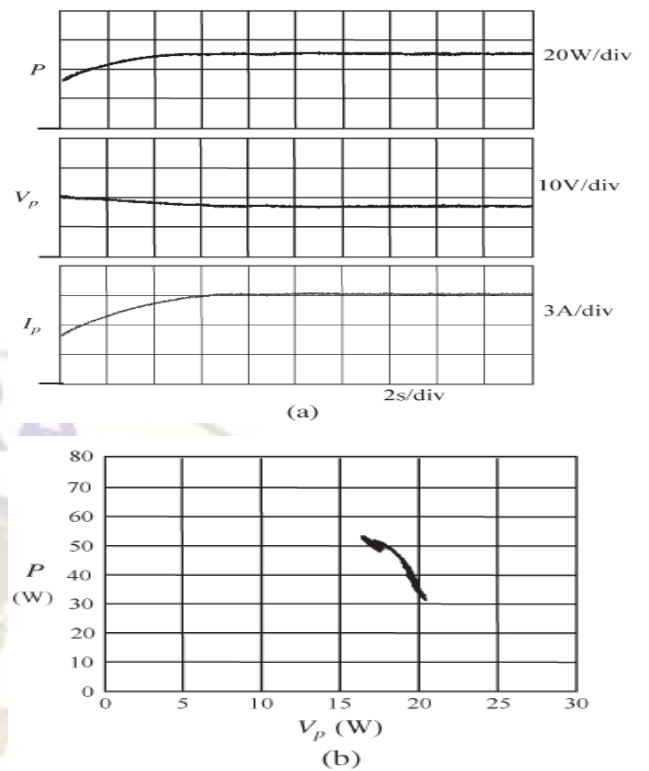


Fig. 13. MPPT response of the charge.

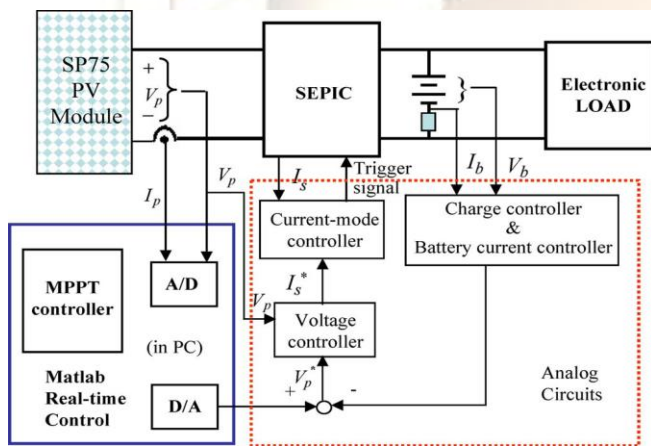


Fig. 12. Implementation of the whole system.

The measured waveforms for demonstrating the power balance feature are shown in Fig. 14. Fig. 14(a) shows that the load power (84 W) is larger than the available PV power (MPPT, 60 W), the insufficient power is supplied by the battery (24W), and the PV module is operated at MPPT. Fig. 14(b) shows that the load power is small and that the PV module discards the MPPT (20 W) to keep the battery charged in constant current (0.6 A). These all demonstrate that the proposed power balance control is effective.

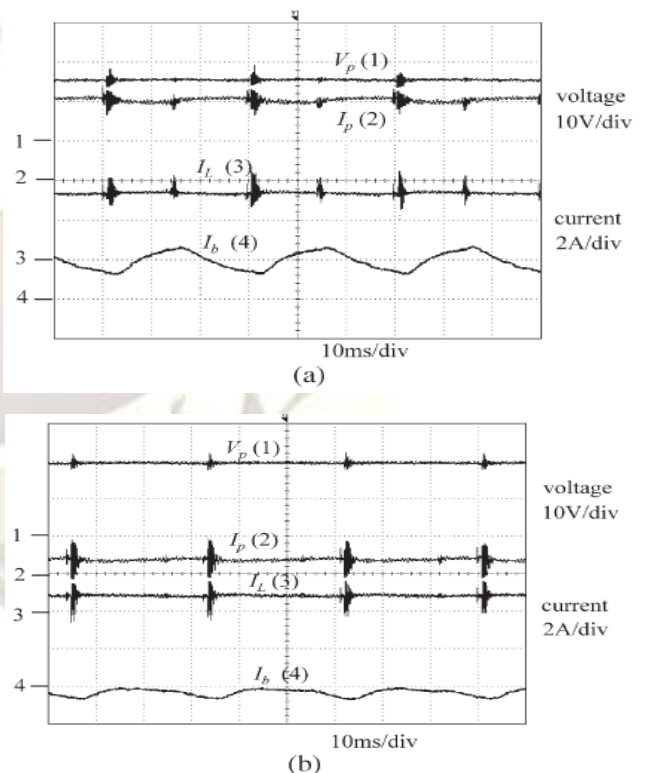


Fig.14. Measured waveforms for demonstrating the power balance feature. (a) Load power is larger than the available PV power. (b) Sum of the load power and the charge power is less than the peak power of the PV module.

V. CONCLUSION

This paper has presented a PV charger implemented with the SEPIC converter. The system has been proved to be effective in the MPPT and power balance control. The proposed modeling method of the converter with the PV module input and peak current- mode control, the adaptive MPPT control method, as well as the power balance control method can also be applied to the charger with other types of converter. The MPPT controller was implemented with the Matlab real-time control in thispaper, and it will be changed to be implemented with the microprocessor or DSP and integrated with the voltage controller and PWM to make the system more practical in the future.

REFERENCES

- [1] M. Rogol, S. Doi, and A. Wilkinson, "Sun screen: Investment opportunities in solar power," *Solar Power Sector Outlook*, Jul. 7, 2004, CLSA Asia-Pacific Markets.
- [2] German Advisory Council on GlobalChange, 2003.
- [3] S. B. Kjaer, J. K. Pedersen, and F. Blaabjerg, "A review of single-phase grid-connected inverters for photovoltaic modules," *IEEE Trans. Ind. Appl.*, vol. 41, no. 5, pp. 1292–1306, Sep./Oct. 2005.
- [4] R. A. Mastromauro, M. Liserre, and A. Dell'Aquila, "Study of the effects of inductor nonlinear behavior on the performance of current controllers for single-phase PV grid converters," *IEEE Trans. Ind. Electron.*, vol. 55, no. 5, pp. 2043–2052, May 2008.
- [5] Y. K. Lo, T. P. Lee, and K. H. Wu, "Grid-connected photovoltaic system with power factor correction," *IEEE Trans. Ind. Electron.*, vol. 55, no. 5, pp. 2224–2227, May 2008.
- [6] H. Koizumi, T. Mizuno, T. Kaito, Y. Noda, N. Goshima, M. Kawasaki, K. Nagasaka, and K. Kurokawa, "A novel microcontroller for grid connected photovoltaic systems," *IEEE Trans. Ind. Electron.*, vol. 53, no. 6, pp. 1889–1897, Dec. 2006.
- [7] W. Xiao, N. Ozog, and W. G. Dunford, "Topology study of photovoltaic interface for maximum power point tracking," *IEEE Trans. Ind. Electron.*, vol. 54, no. 3, pp. 1696–1704, Jun. 2007.
- [8] R. J. Wai, W. H. Wang, and C. Y. Lin, "High-performance stand-alone photovoltaic generation system," *IEEE Trans. Ind. Electron.*, vol. 55, no. 1, pp. 240–250, Jan. 2008.
- [9] F. Liu, S. Duan, F. Liu, B. Liu, and Y. Kang, "A variable step size INC MPPT method for PV systems," *IEEE Trans. Ind. Electron.*, vol. 55, no. 7, pp. 2622–2628, Jul. 2008.
- [10] D. Sera, R. Teodorescu, J. Hantschel, and M. Knoll, "Optimized maximum power point tracker for fast-changing environmental conditions," *IEEE Trans. Ind. Electron.*, vol. 55, no. 7, pp. 2629–2637, Jul. 2008.
- [11] J. H. R. Enslin and D. B. Snyman, "Combined low-cost, high-efficient inverter, peak power tracker and regulator for PV applications," *IEEE Trans. Power Electron.*, vol. 6, no. 1, pp. 73–82, Jan. 1991.
- [12] E. Koutroulis and K. Kalaitzakis, "Novel battery charging regulation systemfor photovoltaic applications," *Proc. Inst. Elect. Eng.—Elect. PowerAppl.*, vol. 151, no. 2, pp. 191–197, Mar. 2004.
- [13] D. Adar, G. Rahav, and S. Ben-Yaakov, "A unified behavioral averagemodel of SEPIC converters with coupled inductors," in *Proc. IEEE PESC*, 1997, pp. 441–446.
- [14] H. Yun, Z. Zhong, Z. Sun, and G. Wan, "Research on power balancestrategy of fuel cell vehicle powertrain," in *Proc. IEEE ICVES*, 2006, pp. 388–393.
- [15] Z. Jiang, "Power management of hybrid photovoltaic—Fuel cell powersystems," in *Proc. IEEE Power Eng. Soc. Gen. Meeting*, 2006, pp. 1–6.
- [16] M. H. Nehrir, C. Wang, and S. R. Guda, "Alternative energy distributedgeneration: Need for multi-source operation," in *Proc. 38th NAPS*, 2006, pp. 547–551.
- [17] Z. Jiang and R. A. Dougal, "Multiobjective MPPT/charging controllerfor standalone PV power systems under different insolation and loadconditions," in *Conf. Rec. IEEE IAS Annu. Meeting*, 2004, pp. 1154–1160.
- [18] *PSIM simulation software*, Powersim Inc.
- [19] R. W. Erickson, *Fundamental of Power Electronics*. Norwell, MA:Kluwer, 1997.
- [20] A. I. Pressman, *Switching Power Supply Design*. New York:Mcgraw-Hill.
- [21] S. E. Mineiro, Jr., S. Daher, F. L. M. Antunes, and C. M. T. Cruz, "Photovoltaicsystem for supply public illumination in electrical energy demandpeak," in *Proc. IEEE APEC*, 2004, pp. 1501–1506.
- [22] L. Wu, Z. Zhao, and J. Liu, "A single-stage three-phase grid-connectedphotovoltaic system with

modified MPPT method and reactive powercompensation,” *IEEE Trans. Energy Convers.*, vol. 22, no. 4, pp. 881–886, Dec. 2007.

- [23] E. Koutroulis, K. Kalaitzakis, and N. C. Voulgaris, “Development of amicrocontroller-based, photovoltaic maximum power point tracking controlsystem,” *IEEE Trans. Power Electron.*, vol. 16, no. 1, pp. 46–54,Jan. 2001.



K.Kishore Reddy was born in kurnool, India. He received the B.Tech (Electrical and Electronics Engineering) degree from the Jawaharlal Nehru Technological University, Anantapur in 2005; M.Tech (Power Electronics) from the Karunya university in 2009. He is currently an Asst. Professor of the Dept. of Electrical and Electronic Engineering, R.G.M College of Engineering and Technology, Nandyal. His area of interest power electronics and Electric Drives.

(E-mail: kishorekamireddy@gmail.com).



A.Giddaiah was born in Kurnool, India. He received the B.Tech (Electrical and Electronics Engineering) degree from the Jawaharlal Nehru Technological University, Anantapur in 2011 and persuing the M.Tech (Power Electronics) from Jawaharlal Nehru Technological University, Anantapur. His area of interest in the field of power electronic converters and Electric Drives. (E-mail: ntdevid@gmail.com).